Nuclear Science and Techniques (2024) 35:207
https://doi.org/10.1007/s41365-024-01574-3

# The large-scale modular BGO detection array (LAMBDA) design and test

Yao-De Sheng[1] · Lu-Yang Song[1] · Jun Su[1] · Shi-Lun Jin[2] · Fei Lu[3] · Yang-Ping Shen[4] · Jun-Feng Chen[5] · Li-Yong Zhang[1] · Jian-Jun He[1,6] · Xin-Yue Li[1,6] · Hong-Na Liu[1] · Feng-Shou Zhang[1] · Meng-Lin Qiu[1] · Shen Lin[1] · Hao Zhang[1] · Luo-Huan Wang[1,7] · Zi-Ming Li[1] · Yin-Ji Chen[1] · Xin-Zhi Jiang[1] · Xin Chen[1] · Zhi-Lin Shen[1] · Feng-Cheng Liu[1] · Zhi-Wei Qin[1] · Lin Wang[1] · Yi-Tong Huang[1] · Xiang Li[5] · Si-Ze Chen[8] · You-Bao Wang[4] · Zhi-Hong Li[4] · Bing Guo[4] · Wei-Ping Liu[4,9]

Received: 26 June 2024 / Revised: 21 July 2024 / Accepted: 29 July 2024 / Published online: 23 October 2024


**Abstract**
Total absorption gamma-ray spectroscopy (TAGS) is a powerful tool for measuring complex $\gamma$ transitions, which has been effectively applied to the study of reactor decay heat. This paper presents the design of a new TAGS detector, the large-scale modular BGO detection array (LAMBDA), tailored for measuring $\beta$-decay intensity distributions of fission products. The modular design allows the LAMBDA detectors to be assembled in various configurations. The final version of LAMBDA consists of 102 identical 60 mm × 60 mm × 120 mm BGO crystals and exhibits a high full-energy peak efficiency exceeding 80% at 0.5~8 MeV based on a Monte Carlo simulation. Currently, approximately half of the LAMBDA modules have been manufactured. Tests using $\gamma$-ray sources and nuclear reactions demonstrated favorable energy resolution, energy linearity, and efficiency uniformity across the modules. Forty-eight modules have been integrated into the prototype LAMBDA-I. The capability of LAMBDA-I in $\beta$-delayed $\gamma$-decay experiments was evaluated by commissioning measurements using the $^{152}$Eu source.

**Keywords** Total absorption gamma-ray spectroscopy · Reactor decay heat · Beta-decay · BGO detector array · LAMBDA

## 1 Introduction

Reactor decay heat refers to the thermal energy released through radioactive decay of fission and neutron transmutation products within a nuclear reactor. Despite the small contribution of decay heat to the thermal output during reactor operation, its role is crucial when the reactor is shut down. Efficient cooling and removal of decay heat are essential for mitigating risks such as overheating or fuel melting. Even after removal from the reactor, spent fuel continues to emit decay heat, which must be adequately cooled during storage and transportation to minimize accidents. Consequently, a comprehensive understanding of the decay heat is essential, which has garnered substantial scientific interest and research efforts [1–3].

Based on abundant nuclear data, the most commonly used method for calculating reactor decay heat is the summation method [4]. Because most fission products are neutron-rich nuclides, $\beta^-$-decay dominates the radioactive decay within the reactor. The energy released by $\beta^-$-decay ($Q_\beta$) is typically carried by electrons, neutrinos, daughter nuclei, and $\gamma$-rays. Decay heat is predominantly deposited by electrons and $\gamma$-rays because the kinetic energy of the daughter nucleus is negligible, and neutrinos easily traverse the reactor without significant energy loss. Consequently, the decay heat contributed by individual radioactive fission products can be estimated using the average $\gamma$ energy $\overline{E}_\gamma$ and average $\beta$ energy $\overline{E}_\beta$ produced per $\beta$-decay [5], which can be calculated using the $\beta$-decay intensity distribution $I_\beta(E_x)$ as follows:

This work was supported by the National Key R&D Program of China (Nos. 2022YFA1603300, 2018YFA0404401, 2023YFA1606701, and 2022YFA1602301), National Natural Science Foundation of China (Nos. U1867211, 12275026, and 12222514), and the CAS Light of West China Program (No. 2020-82).

Extended author information available on the last page of the article

$$\overline{E}_{\gamma} = \int_0^{Q_\beta} I_\beta(E_x) E_x \mathrm{d}E_x, \tag{1}$$

$$\overline{E}_{\beta} = \int_0^{Q_\beta} I_\beta(E_x) \left\langle E_\beta(Q_\beta - E_x) \right\rangle \mathrm{d}E_x. \tag{2}$$

Here $E_x$ is the level energy of the daughter nucleus, and $\left\langle E_\beta(Q_\beta - E_x) \right\rangle$ is the average $\beta$ energy of an individual $\beta$-feeding. Therefore, $I_\beta(E_x)$ is an essential input in the summation method, which must be determined accurately. Additionally, $I_\beta(E_x)$ is significant in the study of reactor antineutrino anomalies [6] and the neutrinoless double-$\beta$ decay [7].

In traditional studies, $I_\beta(E_x)$ is typically derived from the measurements of $\beta$-delayed $\gamma$-decay using high-purity germanium (HPGe) detectors. However, for $\beta$-decays with large $Q_\beta$ values, subsequent $\gamma$ transitions from high states in the daughter nucleus are typically weak and prone to being overlooked in the measurement owing to the limited detection efficiency of HPGe detectors. This limitation results in an inadequate understanding of $I_\beta(E_x)$ as discovered by Hardy et al. [8]. This issue, which is known as the "Pandemonium effect," is a potential factor contributing to the observed discrepancy between decay heat calculated via summation methods and that measured by calorimetric experiments [9, 10].

A recently developed technique known as total absorption gamma-ray spectroscopy (TAGS) [11], provides an effective solution to the Pandemonium effect. TAGS detectors commonly employ scintillators with large volumes as detectors, which significantly enhances the detection efficiency of $\gamma$-rays. The high efficiency of the TAGS detector allows the detection of the total $\gamma$ energy emitted during a single $\beta$-decay event, thereby reducing the risk of overlooking $\gamma$-rays with low branching ratios. TAGS facilitates multiple measurements to refine $I_\beta(E_x)$ of the fission products [12–15], which significantly improves the accuracy of the decay heat summation calculations. In addition, the TAGS technique has been applied in other studies, such as direct measurements of the cross-sections of radioactive capture reactions [16–19], and the $\beta$-Oslo method [20, 21] developed to indirectly investigate the (n,$\gamma$) reaction cross-sections.

However, because TAGS detectors cannot attain the desired detection efficiency of 100% and the resolution is limited, the measured total energy $\gamma$ spectrum of $\beta$-decay cannot directly represent the $\beta$ intensity distribution. Further analysis is required by utilizing the response functions for individual $\beta$-feeding. If the excited state decays directly to the ground state, Monte Carlo simulation can be used to construct the response function. However, when feeding is followed by multiple cascade $\gamma$ transitions, the response function is highly correlated with the multiplicity and energy assignment of the cascade [22]. These factors are often ambiguous, particularly for nuclides far from the stability valley, which leads to significant uncertainties in deriving the $\beta$ intensity distribution.

Several state-of-the-art TAGS detectors have been developed in recent years to improve the precision of the $\beta$ intensity distribution, such as SuN [23], DTAS [24], and MTAS [25–27]. These new TAGS detector devices feature improved detection efficiencies compared with their predecessors, effectively minimizing the impact of cascade modes on the response function. Moreover, the use of detector arrays instead of a single detector enables $\gamma$-$\gamma$ coincidence analysis, facilitating a deeper investigation into the cascade modes involved in the de-excitation of the daughter nucleus.

In this work, we introduce a new TAGS detector called the large-scale modular BGO detection array (LAMBDA), which is specifically designed to measure $\beta$-decay intensity distributions of fission products. Section 2 details the design features of LAMBDA. Section 3 presents the property tests of the completed modules with standard $\gamma$-ray sources. Section 4 introduces the assembly and testing of the prototype LAMBDA-I. Section 5 presents the commissioning measurement of LAMBDA-I utilizing $^{152}$Eu source.

## 2 Design of LAMBDA

Selecting an appropriate scintillator is crucial for achieving high detection efficiency. In most TAGS detector designs, NaI(Tl) scintillators are selected owing to their moderate detection efficiency, energy resolution, and cost-effectiveness. However, the limited attenuation capacity of NaI(Tl) for $\gamma$-rays with energies in the MeV range necessitates the use of large crystals to achieve high efficiency. For example, approximately 1 ton of NaI(Tl) crystals was used to construct MTAS [25, 26]. The increase in crystal size compromises the energy resolution and introduces several experimental challenges, such as the need for larger shields.

In the design of LAMBDA, the BGO scintillator was selected because of its high attenuation capacity for $\gamma$-rays [28]. Compared to NaI(Tl), the BGO material exhibits higher density and effective atomic number. To achieve an equivalent efficiency for 4 MeV $\gamma$-rays, the volume of the BGO crystal should be approximately 15% that of NaI(Tl). Additionally, less encapsulation material is required for manufacturing BGO detectors, reducing $\gamma$-ray attenuation within the non-crystal material because the BGO crystal is non-hygroscopic in air.

As shown in Fig. 1, LAMBDA comprises of 102 identical modules arranged in rectangular shapes. The primary component of each module is a BGO crystal with dimensions of 60 mm×60 mm×120 mm. The thickness of 120 mm ensures high attenuation capacity for $\gamma$-rays in the MeV range. The central hole in the LAMBDA, whose cross-sectional area is 120 mm×120 mm, provides adequate space for accommodating the vacuum chamber, silicon detector, and moving tape collector in $\beta$-decay measurements. Furthermore, six additional modules placed on the two sides of the central hole increase the solid-angle coverage.

The detection efficiencies of LAMBDA were estimated using Monte Carlo simulations with GEANT4 code [29]. In the simulation, only the BGO detector modules were involved with a gap of 3 mm between them. Figure 2 shows the simulated total and full-energy peak efficiencies for single $\gamma$-rays in the range of 0.5 to 8 MeV, assuming a point source positioned at the center of LAMBDA. The total efficiencies remain flat and exceed 92% across the entire energy range. The full-energy efficiencies decrease rapidly with increasing $\gamma$ energy from 0.5 to 3 MeV and stabilize at approximately 83% at higher energies.

In the actual $\beta$-decay measurements, the position of $\gamma$ emitter is not confined to a single point. To investigate the influence of the source position on the detection efficiency, the efficiencies of 4 MeV $\gamma$-rays emitted from various positions along the $Y$-axis shown in Fig. 1 were simulated using GEANT4. As shown in Fig. 3, the variation in the efficiency within ±5 cm is less than 2%. The dip observed around the central position originates from the gap between the BGO modules. The typical beam spot size in the decay experiment is approximately ±2 cm, leading to an uncertainty of ∼ 1% in the efficiency.

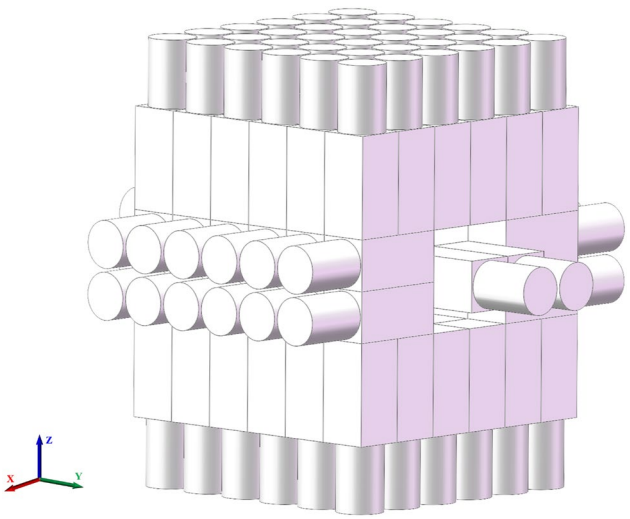

**Fig. 1** (Color online) LAMBDA design scheme consisting of 102 modules. Each module has a BGO crystal with dimensions of 60 mm×60 mm×120 mm coupled to a 2-inch photomultiplier tube (PMT)

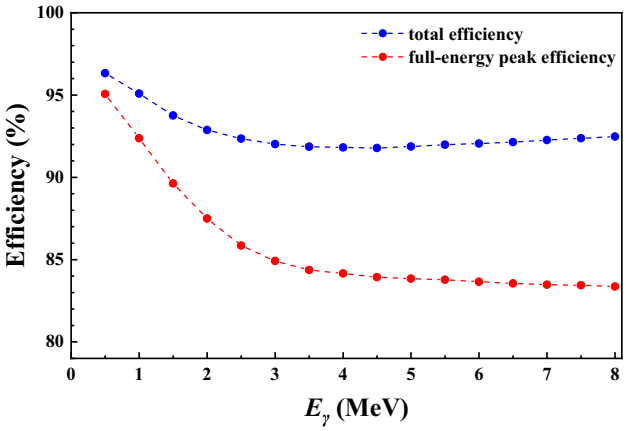


**Fig. 2** (Color online) Monte Carlo simulated efficiency of the LAMBDA in the 0.5 ∼8 MeV energy range. The upper (blue) and lower (red) curves present the total and full-energy peak efficiencies, respectively

## 3 Fabrication and test of the modules

To date, 60 BGO crystals have been fabricated at the Shanghai Institute of Ceramics, Chinese Academy of Sciences (SICCAS) [30]. The following process was adopted while fabricating the crystals into modules. One of the 60 mm×60 mm surfaces of the BGO crystal was polished to serve as the light output end, whereas the other sides were frosted to enhance photon diffuse reflection. A 2-inch PMT (CR173-1) was coupled to the BGO crystal using EJ-550 silicone grease to collect and convert the scintillation photons. Except for the light output area, the

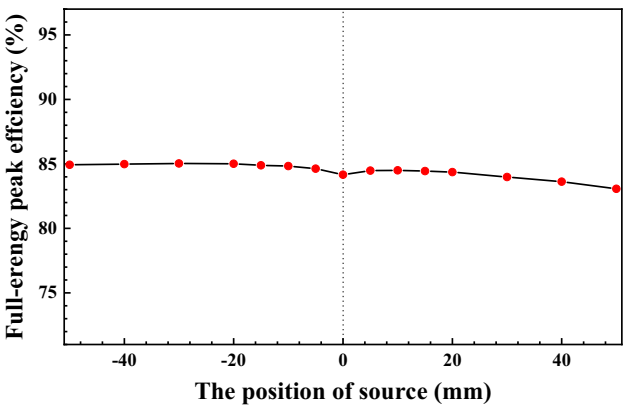


**Fig. 3** (Color online) Full-energy peak efficiency of the LAMBDA detector obtained for 4 MeV $\gamma$-rays versus the position of the source along the Y-axis shown in Fig. 1

surfaces of the BGO crystals were coated using a 65 $\mu$m enhanced specular reflector (ESR) foil (3 M Corporation) to increase light reflection efficiency. The BGO crystal was then installed within a 1-mm-thick carbon fiber housing that served as a light shield and provided mechanical protection. Furthermore, the low atomic number of carbon helped minimize the $\gamma$ attenuation effect of the housing.

To examine the performance of the modules and evaluate their consistency, an initial batch of 50 modules was tested using the $^{137}$Cs $\gamma$ source. As illustrated in Fig. 4, at room temperature, the energy resolutions of the modules at 662 keV range from 9.3 to 10.3%, with an average value of 9.8%, which is worse than the typical value of 7∼8% for 3-inch NaI(Tl) detectors. Because the light yield of BGO crystals increases with decreasing temperature [31–33], we employed a cooling method to improve the energy resolution of the BGO modules. This cooling method has been successfully used in a previous study [16]. Consequently, 30 modules were cooled to −20 °C, yielding an improved average energy resolution of 8.3%, as shown in Fig. 4. This energy resolution is comparable to the typical value for NaI(Tl) of a similar size.

The detection efficiency of each detector module was evaluated using a $^{137}$Cs $\gamma$ source as shown in Fig. 5. The average full-energy peak efficiencies are 1.45% and 0.69% at distances of 100 mm and 200 mm between the source and detector modules, respectively. The results are consistent with the values of 1.46% and 0.69% obtained from the GEANT4 simulations. Furthermore, the standard deviations of the efficiency for the 50 modules were 0.014% and 0.008% at distances of 100 mm and 200 mm, respectively, exhibiting good consistency in the full-energy peak efficiency across all modules.

The energy nonlinearity effect [34] of the module within the 1∼12 MeV range was evaluated using $\gamma$-rays emitted

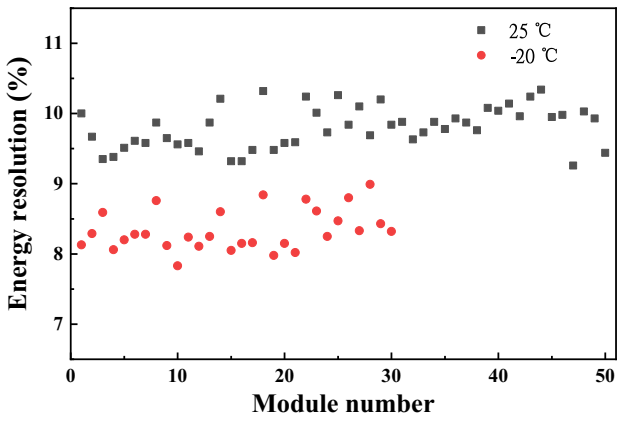


**Fig. 4** (Color online) Energy resolutions of BGO modules measured at 25 °C (black squares) and −20 °C (red circles) for the 662 keV $\gamma$ -ray

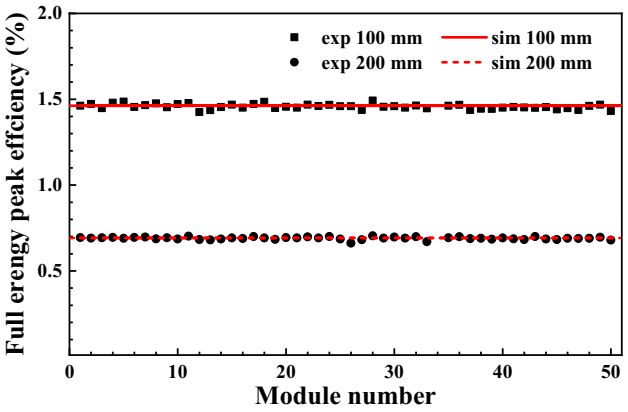


**Fig. 5** (Color online) Full-energy peak efficiency of the BGO module for 662 keV $\gamma$-rays at 100 mm (black squares) and 200 mm (black circles) distances. The solid and dashed red curves indicate the corresponding simulated results

by both natural radioactive isotopes (1.46 MeV from $^{40}$K and 2.61 MeV from $^{208}$Tl) and nuclear reactions (1.78 MeV, 4.50 MeV, 10.02 MeV, and 11.80 MeV from $^{27}$Al(p,$\gamma$)$^{28}$Si and 6.13 MeV from $^{19}$F(p,$\alpha\gamma$)$^{16}$O). A linear fit yielded a goodness-of-fit value of $R^2 = 0.99998$, indicating a maximum deviation of 30 keV in the 1∼12 MeV range.

## 4 Assembly and test of LAMBDA-I

Owing to the limited number of modules currently available, a simplified version of LAMBDA, referred to as LAMBDA-I, was proposed. Figure 6 illustrates the configuration of LAMBDA-I, which comprises 48 BGO modules. LAMBDA-I preserves the essential detection components of LAMBDA, maintaining solid angle coverage of nearly $4\pi$.

The data acquisition system of LAMBDA-I utilized Pixie-16 modules from XIA Inc. [35] to record the experimental data. These modules operated at a sampling frequency of 100 MHz with 14-bit precision. Data were acquired through independent self-triggered channels with timestamps, enabling event reconstruction using software based on preset coincidence windows. EHS F060p modules (ISEG Inc.) were used to supply high voltage to the 48 PMTs. Fine adjustments of the high voltage of each channel aligned the characteristic $\gamma$ peaks of the spectrum from each BGO module, thus minimizing discrepancies in the energy calibrations.

The performance of LAMBDA-I was evaluated by measuring the $\gamma$-rays emitted from $^{137}$Cs and $^{60}$Co point sources positioned at the central position. Figure 7 shows the obtained sum spectra representing the sum energy of all triggered modules. The 2505 keV sum peak of $^{60}$Co $\beta$

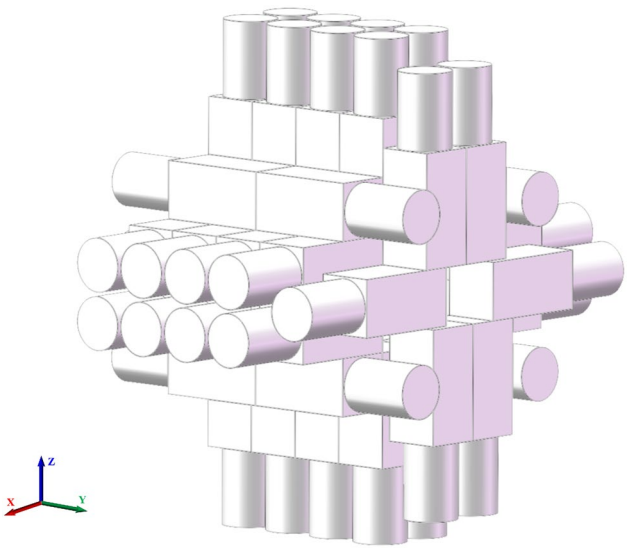

**Fig. 6** (Color online) LAMBDA-I structure scheme consisting of 48 completed modules

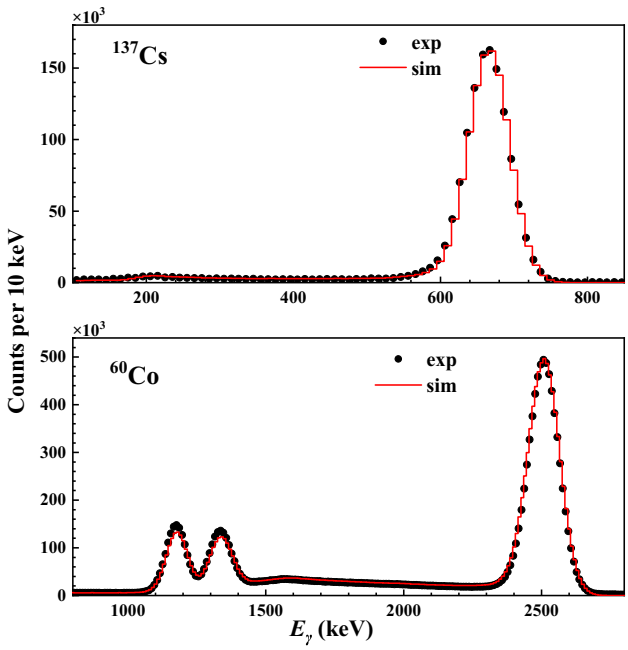


**Fig. 7** (Color online) Comparison of the sum $\gamma$ spectra of $^{137}$Cs and $^{60}$Co sources measured by LAMBDA-I (black circles) with GEANT4 simulations (red curves)

-decay, which corresponds to the total energy released by the de-excitation of the 2505 keV level in $^{60}$Ni, is observed. The presence of weak $\gamma$ peaks at 1173 and 1332 keV indicates the insufficient detection efficiency of LAMBDA-I, corresponding to the escape of one of the two $\gamma$-rays from LAMBDA-I without any energy deposit. The energy resolutions of LAMBDA-I are 10.1%, 7.3%, 6.9%, and 5.2% at 662 keV, 1173 keV, 1332 keV, and 2505 keV, respectively. The full-energy peak efficiencies are (82.5 ± 1.5)% and (50.6 ± 1.2)% for the 662 keV sum peak of $^{137}$Cs and 2505 keV sum peak of $^{60}$Co, respectively.

The determination of the response function of LAMBDA-I is crucial for deconvolving the $\gamma$ spectrum and is typically achieved through Monte Carlo simulations. As shown in Fig. 7, the GEANT4 simulations accurately reproduce the experimental results. The full-energy peak efficiencies obtained from the GEANT4 simulation were 82.8% and 50.9% for the sum peaks of $^{137}$Cs and $^{60}$Co, respectively, which are consistent with the measured values.

The $\gamma$-$\gamma$ coincidence method is a promising technique for resolving unknown cascade transitions in the $\beta$-decay daughter nucleus. Figure 8 presents a two-dimensional plot of the total energy versus the single-module energy measured using the $^{60}$Co source. A 1332–1173 keV cascade transition is identified, indicating that LAMBDA-I is capable of cascade transition analysis. As the 1332–1173 keV cascade transition accounts for 99.9% of the de-excitation of the 2505 keV state in $^{60}$Ni, events falling below the line with a total energy of 2505 keV are primarily caused by incomplete measurement of the total energy. Such tailing effects originating from high levels introduce a remarkable background to the data analysis of lower levels, particularly when the $\beta$-feedings to high-energy levels are strong. Therefore, further improvements in both the detection efficiency and energy resolution are desired.

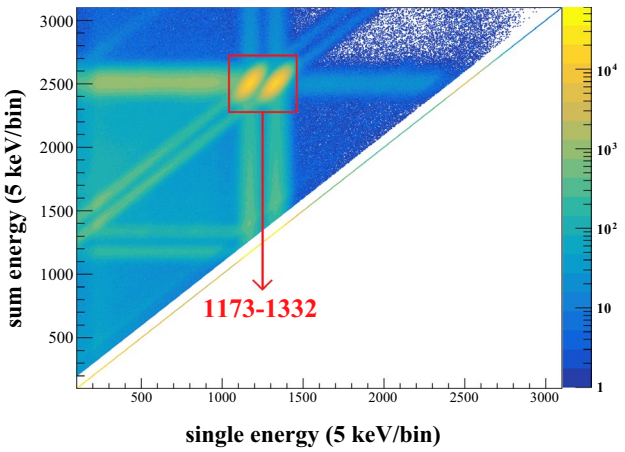


**Fig. 8** (Color online) Two-dimensional spectra of the sum energy vs single energy of $^{60}$Co source from LAMBDA-I. The 1332–1173 keV cascade transition is indicated

## 5 Gamma source commissioning of LAMDBA-I

To estimate the accuracy and uncertainty of LAMBDA-I during measurement of the complex $\beta$-delayed $\gamma$-decay, a commissioning experiment was performed using the $^{152}$Eu source. $^{152}$Eu has two decay modes [36]: electron capture (EC) to $^{152}$Sm with a branching ratio of 72.08% and $\beta^-$-decay to $^{152}$Gd with a branching ratio of 27.92%. The $\beta^+$-decay of $^{152}$Eu is very weak (0.03%) and can be neglected in the analysis. According to the ENSDF database [37], EC and $\beta^-$-decay of $^{152}$Eu can feed 12 states in $^{152}$Gd and 21 states in $^{152}$Sm, respectively. The complexity of $^{152}$Eu decay is comparable to that of fission products.

In the measurement, the $^{152}$Eu source was positioned at the center of LAMBDA-I. The activity of the source was approximately $3.7 \times 10^4$ Bq. To analyze the obtained data, the coincidence window was set to $\pm$300 ns. Figure 9 shows the sum and single spectra of $^{152}$Eu measured using LAMBDA-I. The rapid decline observed at approximately 1.7 MeV in the sum spectrum is caused by the decay energy of EC ($Q_{\mathrm{EC}} = 1.874$ MeV) and $\beta^-$-decay ($Q_{\beta^-} = 1.819$ MeV). Counts in the higher-energy region mainly arise from the natural background and pileup effects. Unlike the sum spectrum, the single spectrum is the superposition of the $\gamma$ spectra measured by each detector module.

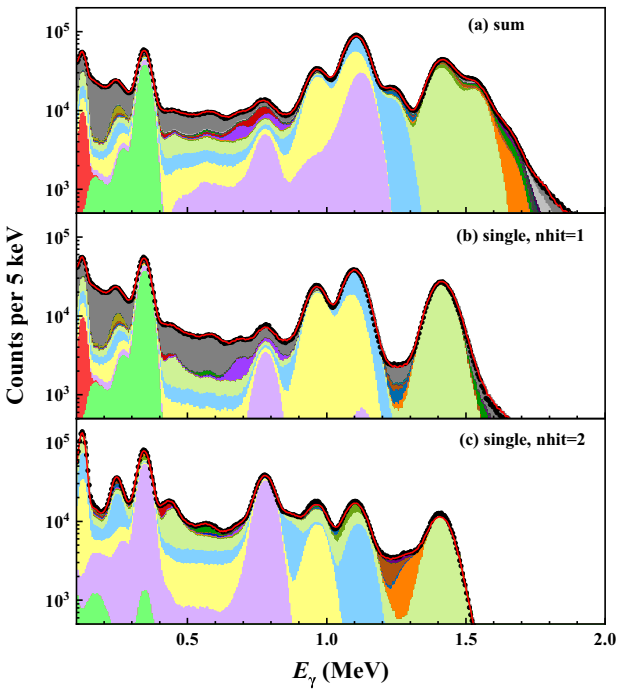


**Fig. 9** (Color online) Spectra of $^{152}$Eu decay obtained by LAMBDA-I, including (a) sum spectrum, (b) single spectrum gated with nhit=1, and (c) single spectrum gated with nhit=2. The dark and light gray shadows indicate the natural background and pileup part, respectively. The rainbow palette shadow represents the fitted response function of each branch of $^{152}$Eu decay. The red curve represents the total contribution of all the branches, natural background, and pileup effect

The branching ratio of $\beta$feeding to each state in the daughter nucleus can be extracted using its relation with the TAGS-measured total energy spectrum:

$$D_i = N \sum_{k=0}^{k_{\max}} b_k R_{ik}, \tag{3}$$

where $D_i$ represents the count of the $i$th channel in the measured spectrum; $N$ is the total number of decays; $b_k$ is the branching ratio of $\beta$-feeding to the $k$th level in the daughter nucleus; and $R_{ik}$ is the response function of TAGS to the $k$th $\beta$-feeding.

Among the levels in $^{152}$Sm and $^{152}$Gd fed by the $\beta$-decay of $^{152}$Eu, several exhibit similar excited energies, such as the 1023 keV, 1085 keV, 1109 keV, and 1123 keV states. The feeding of these adjacent states cannot be distinguished in the sum spectrum because of the limited energy resolution of LAMBDA-I, which results in significant uncertainties in the branching ratio analysis. Fortunately, the multiplicities and individual $\gamma$ energies of the transitions from these levels to the ground state are often different. Therefore, these adjacent levels may be separated using the number of triggered modules in LAMBDA-I (nhit) and the corresponding single spectrum. In this approach, the experimental data were classified into three types of spectra [38], the sum spectrum ($D_{ik}^{\mathrm{sum}}$), single spectrum gated with nhit=1 ($D_{ik}^{\mathrm{single,nhit=1}}$), and single spectrum gated with nhit=2 ($D_{ik}^{\mathrm{single,nhit=2}}$), as shown in Fig. 9.

The response function $R_{ik}$ was extracted from the GEANT4 simulation for each $\beta$-feeding. In the simulation, the $\beta$ energy spectrum and subsequent $\gamma$ transitions for each $\beta$-feeding were generated using the Radioactive-Decay−5.6 library [39] within the GEANT4 code. The number of simulated events for each branch was set to $10^6$. The simulated data were then convoluted using the experimental energy resolution and used for constructing the corresponding $R_{ik}$. Consistent with the analysis of the experimental spectra, the corresponding response functions $R_{ik}^{\mathrm{sum}}$, $R_{ik}^{\mathrm{single,nhit=1}}$, and $R_{ik}^{\mathrm{single,nhit=2}}$ were constructed.

The Bayesian Analysis Toolkit [40] (BAT), which is based on Bayesian theory and executed via Markov Chain Monte Carlo (MCMC) simulations, was adopted to solve Eq. 3. In the analysis, feedings with branching ratios below 0.05% were omitted because of their negligible impact on the data analysis. The natural background and pileup effects were introduced into the analysis as individual and fixed components. The background spectrum was obtained under the same conditions but without the $^{152}$Eu source and was

**Table 1** (Color online) $\beta$ intensities of $^{152}$Eu determined by LAMBDA-I in comparison with ENSDF data

| Daughter nuclei | $\beta$-feeding state (keV) | This work | ENSDF [37] |
|---|---|---|---|
| $^{152}$Gd | 344.2 | 7.88(34)% | 8.25(19)% |
| | 755.4 | 0.96(4)% | 0.91(1)% |
| | 930.6 | 0.15(5)% | 0.284(6)% |
| | 1109.2 | – | 0.264(9)% |
| | 1123.2 | 13.95(44)% | 13.74(9)% |
| | 1434 | 2.31(10)% | 2.43(2)% |
| | 1605.6 | 0.57(32)% | 0.107(2)% |
| | 1643.4 | 1.68(11)% | 1.83(1)% |
| $^{152}$Sm | 121.8 | 2.58(15)% | 1.60(50)% |
| | 366.5 | 0.62(5)% | 0.85(4)% |
| | 810.5 | 1.09(9)% | 1.18(1)% |
| | 1023.0 | – | 0.233(4)% |
| | 1041.1 | – | 0.067(7)% |
| | 1085.8 | 20.22(88)% | 21.50(11)% |
| | 1233.8 | 18.19(79)% | 17.09(8)% |
| | 1292.8 | 0.32(18)% | 0.625(8)% |
| | 1371.7 | 1.22(6)% | 0.85(2)% |
| | 1529.8 | 24.69(75)% | 24.78(11)% |
| | 1579.4 | 1.76(8)% | 2.08(1)% |
| | 1649.8 | 1.12(5)% | 0.93(1)% |
| | 1730.2 | 0.47(16)% | 0.054(3)% |
| | 1757.0 | 0.09(6)% | 0.054(2)% |
| | 1769.1 | 0.13(7)% | 0.082(2)% |
| $\bar{E}_\gamma$ (keV) | | 1178(22) | 1177(3) |

normalized according to the measurement time. The pileup spectrum was constructed by convolving the sum spectrum with itself, based on the count rate and coincidence window width. Owing to the small likelihood of two $\gamma$-rays simultaneously hitting the same module, the pileup effects in the single spectra were minimal and therefore neglected, as shown in Fig. 9(b), (c).

The fitting results for BAT are shown in Fig. 9, in which the contribution of each feeding branch is indicated by a rainbow shadow. The combined contributions from all the branches, the natural background, and the pileup (red curve) are consistent with the experimental data. Table 1 lists the branching ratios of $^{152}$Eu decay obtained, comparing with those recommended in ENSDF [37]. The sources of uncertainty include a simulation of the LAMBDA response function of 3%, an experimental coincidence window width of 1%, a pileup effect of 2%, and the statistical error of the BAT code. The present results are consistent with the ENSDF data within the uncertainties, except for a few levels.

The average $\gamma$ energy of the $^{152}$Eu decay is derived as $(1178 \pm 22)$ keV using the branching ratios obtained in the present work, which is in good agreement with the value $(1177 \pm 3)$ keV calculated using the ENSDF data [37]. The 22 keV uncertainty mostly arises from the error in the branching ratio owing to the small uncertainty in the level energy, which is in the current state-of-the-art [3]. The consistency of the present results and ENSDF data demonstrates the capability of LAMBDA-I to study the $\beta$ intensity and decay heat.

## 6 Summary

This study introduces a novel design for a TAGS detector, named LAMBDA, for measuring the $\beta$-decay intensity distributions of fission products. The final version of LAMBDA, comprising 102 BGO modules, achieved full-energy peak efficiency in the current state-of-the-art. LAMBDA-I, which consisted of 48 BGO modules, was tested using a $^{152}$Eu source. The $\beta$ intensities of $^{152}$Eu decay were derived using the BAT code with response functions constructed through GEANT4 simulations. The obtained average $\gamma$ energy was consistent with the value derived from the ENSDF data, demonstrating the capability of LAMBDA-I to study $\beta$ intensity and decay heat. Currently, LAMBDA-I is installed at the Beijing Radioactive Ion-beam Facility (BRIF) [41, 42] and is used to measure the $\beta$-decay intensity of fission products. To provide advanced equipment for decay heat studies, future efforts will focus on producing the remaining BGO modules and assembling the final version of the LAMBDA.

**Author Contribution** All authors contributed to the study conception and design. LAMBDA was designed by Jun Su and Yao-De Sheng. LAMBDA detector and BGO modules developed by Jun Su, Yao-De Sheng, Shi-Lun Jin, Fei Lu, Yang-Ping Shen and Jun-Feng Chen. Experiment was carried out by Yao-De Sheng, Jun Su, Lu-Yang Song, Li-Yong Zhang, Xin-Yue Li, Shen Lin, Hao Zhang, Luo-Huan Wang, Zi-Ming Li, Yin-Ji Chen, Xin-Zhi Jiang, Xin Chen, Zhi-Lin Shen, Feng-Cheng Liu, Zhi-Wei Qin, Lin Wang and Yi-Tong Huang. Data analysis was performed by Yao-De Sheng and Lu-Yang Song. The first draft of the manuscript was written by Yao-De Sheng and all authors commented on previous versions of the manuscript. All authors read and approved the final manuscript.

**Data availability** The data that support the findings of this study are openly available in Science Data Bank at https://cstr.cn/31253.11.sciencedb.j00186.00330 and https://doi.org/10.57760/sciencedb.j00186.00330

## Declarations

**Conflict of interest** Feng-Shou Zhang and Wei-Ping Liu are the editorial board members for Nuclear Science and Techniques and were not involved in the editorial review, or the decision to publish this article. All authors declare that there is no conflict of interest.

## References


1. A. Tobias, Decay heat. Prog. Nucl. Energ. **5**, 1–93 (1980). https://doi.org/10.1016/0149-1970(80)90002-5
2. M.A. Kellett, A.L. Nichols, Assessment of fission product decay data for decay heat calculations. Nucl. Sci. NEA/WPEC-25 Report **6284**, 1 (2007)
3. A.L. Nichols, P. Dimitriou, A. Algora et al., Improving fission-product decay data for reactor applications: part I-decay heat. Eur. Phys. J. A **59**, 4 (2023). https://doi.org/10.1140/epja/s10050-023-00969-x
4. T. Yamamoto, K. Sugiyama, Summation calculations of fission-product decay heat, their uncertainties and their applications to a fast breeder reactor. Ann. Nucl. Energy **5**, 621 (1978). https://doi.org/10.1016/0306-4549(78)90036-1
5. T. Yoshida, R. Nakasima, Decay heat calculations based on theoretical estimation of average beta- and gamma-energies released from short-lived fission products. J. Nucl. Sci. Technol. **18**, 393 (1981). https://doi.org/10.1080/18811248.1981.9733273
6. C. Bemporad, G. Gratta, P. Vogel, Reactor-based neutrino oscillation experiments. Rev. Mod. Phys. **74**, 297 (2002). https://doi.org/10.1103/revmodphys.74.297
7. J.D. Vergados, H. Ejiri, F. Šimkovic, Theory of neutrinoless double-beta decay. Rep. Prog. Phys. **75**, 297 (2012). https://doi.org/10.1088/0034-4885/75/10/106301
8. J. Hardy, L.C. Carraz, B. Jonson et al., The essential decay of pandemonium: a demonstration of errors in complex beta-decay schemes. Phys. Lett. B **71**, 307 (1977). https://doi.org/10.1016/0370-2693(77)90223-4
9. J.K. Dickens, T.A. Love, J.W. McConnell et al., Fission-product energy release for times following thermal-neutron fission of $^{235}$U between 2 and 14000 s. Nucl. Sci. Eng. **74**, 106 (1980). https://doi.org/10.13182/NSE80-A19627
10. J.K. Dickens, T.A. Love, J.W. McConnell et al., Fission-product energy release for times following thermal-neutron fission of Plutonium-239 and Plutonium-241 between 2 and 14000 s. Nucl. Sci. Eng. **78**, 126 (1981). https://doi.org/10.13182/NSE81-A20099
11. R.C. Greenwood, D.A. Struttmann, K.D. Watts, Use of a total absorption gamma-ray spectrometer to measure ground-state beta-branching intensities. Nucl. Instrum. Methods A **390**, 514 (1992). https://doi.org/10.1016/0168-9002(92)90607-6
12. R.C. Greenwood, R.G. Helmer, M.H. Putnam et al., Measurement of beta-decay intensity distributions of several fission-product isotopes using a total absorption gamma-ray spectrometer. Nucl. Instrum. Methods A **390**, 95 (1997). https://doi.org/10.1016/S0168-9002(97)00356-2
13. B. Rubio, E. Nácher, A. Algora et al., Beta decay studies far from stability with the total absorption technique: the case of $^{76}$Sr. Nucl. Phys. A **752**, 251 (2005). https://doi.org/10.1016/j.nuclphysa.2005.02.147
14. M. Karny, J.M. Nitschke, L.F. Archambault et al., Coupling a total absorption spectrometer to the GSI on-line mass separator. Nucl. Instrum. Methods B **126**, 411 (1997). https://doi.org/10.1016/S0168-583X(96)01007-5
15. A. Algora, D. Jordan, J.L. Tain et al., Reactor decay heat in $^{239}$Pu: solving the $\gamma$ discrepancy in the 4–3000 s cooling period. Phys. Rev. Lett. **105**, 202501 (2010). https://doi.org/10.1103/PhysRevLett.105.202501
16. J. Su, H. Zhang, Z.H. Li et al., First result from the Jinping Underground Nuclear Astrophysics experiment JUNA: precise measurement of the 92 keV $^{25}$Mg(p, $\gamma$)$^{26}$Al resonance. Sci. Bull. **67**, 125 (2021). https://doi.org/10.1016/j.scib.2021.10.018
17. L.Y. Zhang, J. Su, J.J. He et al., Direct measurement of the astrophysical $^{19}$F(p, $\alpha\gamma$)$^{16}$O reaction in the Deepest Operational Underground Laboratory. Phys. Rev. Lett. **127**, 152702 (2021). https://doi.org/10.1103/PhysRevLett.127.152702
18. L.Y. Zhang, J.J. He, R.J. deBoer et al., Measurement of $^{19}$F (p, $\gamma$)$^{20}$Ne reaction suggests CNO breakout in Eso Astrophy Symp. Nature **656**, 152702 (2022). https://doi.org/10.1038/s41586-022-05230-x
19. L.H. Wang, J. Su, Y.P. Shen et al., Measurement of the $^{18}$O($\alpha$, $\gamma$)$^{22}$Ne reaction rate at JUNA and its impact on probing the origin of SiC grains. Phys. Rev. Lett. **130**, 092701 (2023). https://doi.org/10.1103/PhysRevLett.130.092701
20. A.C. Larsen, S.N. Liddick, A. Spyrou et al., The Beta-Oslo Method: experimentally constrained (n, $\gamma$) reaction rates relevant to the r-Process. Nuclei Cosmos XV **219**, 137 (2019). https://doi.org/10.1007/978-3-030-13876-9-22
21. G.C. Yang, L.M. Hua, F. Lu et al., Response functions of a 4$\pi$ summing gamma detector in Beta-Oslo method. Nucl. Sci. Tech. **33**, 68 (2022). https://doi.org/10.1007/s41365-022-01058-2
22. J.L. Tain, D. Cano-Ott, The influence of the unknown de-excitation pattern in the analysis of beta-decay total absorption spectra. Nucl. Instrum. Methods A **571**, 719 (2007). https://doi.org/10.1016/j.nima.2006.09.084
23. A. Simon, S.J. Quinn, A. Spyrou et al., SuN: summing NaI(Tl) gamma-ray detector for capture reaction measurements. Nucl. Instrum. Methods A **703**, 16 (2013). https://doi.org/10.1016/j.nima.2012.11.045
24. V. Guadilla, A. Algora, J.L. Tain et al., First experiment with the NUSTAR/FAIR decay total absorption gamma-Ray spectrometer (DTAS) at the IGISOL IV facility. Nucl. Instrum. Methods B **376**, 334 (2016). https://doi.org/10.1016/j.nimb.2015.12.018
25. B.C. Rasco, A. Fijałkowska, M. Karny et al., The nonlinear light output of NaI(Tl) detectors in the modular total absorption spectrometer. Nucl. Instrum. Methods A **788**, 137 (2015). https://doi.org/10.1016/j.nima.2015.03.087
26. M. Karny, K.P. Rykaczewski, A. Fijałkowska et al., Modular total absorption spectrometer. Nucl. Instrum. Methods A **836**, 83 (2016). https://doi.org/10.1016/j.nima.2016.08.046
27. M. Karny, A. Fijałkowska, R.K. Grzywacz et al., Design of a new central module for the modular total absorption spectrometer. Nucl. Instrum. Methods B **463**, 390 (2019). https://doi.org/10.1016/j.nimb.2019.04.045
28. C.E. Moss, E.J. Dowdy, M.C. Lucas, Bismuth germanate scintillators: applications in nuclear safeguards and Health Phys. Nucl. Instrum. Methods A **242**, 480 (1986). https://doi.org/10.1016/0168-9002(86)90450-X
29. S. Agostinelli, J. Allison, K. Amako et al., Geant4-a simulation toolkit. Nucl. Instrum. Methods A **506**, 250 (2003). https://doi.org/10.1016/S0168-9002(03)01368-8
30. Z.M. Ji, H.H. Ni, L.Y. Yuan et al., Investigation of optical transmittance and light response uniformity of 600-mm-long BGO crystals. Nucl. Instrum. Methods A **753**, 143 (2014). https://doi.org/10.1016/j.nima.2014.03.056
31. J. Gironnet, V.B. Mikhailik, H. Kraus et al., Scintillation studies of Bi4Ge3O12 (BGO) down to a temperature of 6K. Nucl. Instrum. Methods A **594**, 358 (2008). https://doi.org/10.1016/j.nima.2008.07.008
32. P.L. Wang, Y.L. Zhang, Z.Z. Xu et al., Study on the temperature dependence of BGO light yield. Sci. China Phys. Mech. Astron. **57**, 1898 (2014). https://doi.org/10.1007/s11433-014-5548-4
33. M. Moszynski, M. Balcerzyk, W. Czarnacki et al., Intrinsic energy resolution and light yield nonproportionality of BGO. IEEE T. Nucl. Sci. **51**, 1074 (2004). https://doi.org/10.1109/TNS.2004.829491
34. T.D. Taulbee, B.D. Rooney, W. Mengesha et al., The measured electron response nonproportionality of $CaF_2$, BGO, LSO, and GSO. IEEE Nucl. Sci. Symp. Conf. Rec. **1**, 326 (1996). https://doi.org/10.1109/NSSMIC.1996.590969

35. xia.com/support/pixie-16.html
36. M.J. Martin, Nuclear data sheets for A = 152. Nucl. Data Sheets **114**, 1479 (2013). https://doi.org/10.1016/j.nds.2013.11.001
37. National Nuclear Data Center, NuDat database (1996), https://www.nndc.bnl.gov/nudat Accessed 20 Feb 2024
38. J.R. Dermigny, C. Iliadis, M.Q. Buckner et al., Gamma-ray spectroscopy using a binned likelihood approach. Nucl. Instrum. Methods A **830**, 427 (2016). https://doi.org/10.1016/j.nima.2016.06.017
39. S. Hauf, M. Kuster, M. Batič et al., Radioactive decays in Geant4. IEEE Trans. Nucl. Sci. **60**, 2966 (2013). https://doi.org/10.1109/TNS.2013.2270894
40. A. Caldwell, D. KollSSr, K. Kröninger, BAT—the Bayesian analysis toolkit. Comput. Phys. Commun. **180**, 2197 (2009). https://doi.org/10.1016/j.cpc.2009.06.026
41. W.P. Liu, Z.H. Li, X.X. Bai et al., BRIF and CARIF progress. Sci. China Phys. Mech. Astron. **54**, 14 (2011). https://doi.org/10.1007/s11433-011-4422-x
42. B. Tang, B.Q. Cui, L.H. Chent et al., The development of the FEBIAD ion source for BRISOL. Nucl. Instrum. Methods B **463**, 154 (2020). https://doi.org/10.1016/j.nimb.2019.06.003



## Authors and Affiliations

**Yao-De Sheng[1] · Lu-Yang Song[1] · Jun Su[1] · Shi-Lun Jin[2] · Fei Lu[3] · Yang-Ping Shen[4] · Jun-Feng Chen[5] · Li-Yong Zhang[1] · Jian-Jun He[1,6] · Xin-Yue Li[1,6] · Hong-Na Liu[1] · Feng-Shou Zhang[1] · Meng-Lin Qiu[1] · Shen Lin[1] · Hao Zhang[1] · Luo-Huan Wang[1,7] · Zi-Ming Li[1] · Yin-Ji Chen[1] · Xin-Zhi Jiang[1] · Xin Chen[1] · Zhi-Lin Shen[1] · Feng-Cheng Liu[1] · Zhi-Wei Qin[1] · Lin Wang[1] · Yi-Tong Huang[1] · Xiang Li[5] · Si-Ze Chen[8] · You-Bao Wang[4] · Zhi-Hong Li[4] · Bing Guo[4] · Wei-Ping Liu[4,9]**

✉ Jun Su
sujun@bnu.edu.cn

✉ Shi-Lun Jin
jinshilun@impcas.ac.cn

✉ Fei Lu
lufei@sari.ac.cn

1 Key Laboratory of Beam Technology of Ministry of Education, School of Physics and Astronomy, Beijing Normal University, Beijing 100875, China

2 Institute of Modern Physics, Chinese Academy of Sciences, Lanzhou 730000, China

3 Shanghai Advanced Research Institute, Chinese Academy of Sciences, Shanghai 201210, China

4 China Institute of Atomic Energy, P. O. Box 275(10), Beijing 102413, China

5 Shanghai Institute of Ceramics, Chinese Academy of Sciences, Shanghai 201800, China

6 Key Laboratory of Nuclear Physics and Ion-Beam Application (MoE), Institute of Modern Physics, Fudan University, 200433 Shanghai, China

7 School of Mathematics and Physics, Handan University, Handan 056005, China

8 Institute of Nuclear Energy Safety Technology, Hefei Institutes of Physical Science, Chinese Academy of Sciences, Hefei 230031, China

9 Department of Physics, Southern University of Science and Technology, Shenzhen 518055, China